Chemical Physics Impact 10 (2025) 100847

Contents lists available at ScienceDirect

Chemical Physics Impact

journal homepage: www.sciencedirect.com/journal/chemical-physics-impact

Full Length Article

Fabrication of highly sensitive room temperature operated NO_2 gas sensor using back gated 2D-MoS_2 FETs

Sujit Kumar [a], Anjali Sharma [b,*], Ajay K. Sao [c,d], Jatinder Pal Singh [c,d], Arijit Chowdhuri [c,d], Monika Tomar [e]

[a] IMEC, 3001, Leuven, Belgium
[b] Department of Physics, Atma Ram Sanatan Dharma College, University of Delhi, Delhi, 110021, India
[c] Department of Physics and Astrophysics, University of Delhi, Delhi, 110007, India
[d] Department of Physics, Acharya Narendra Dev College (University of Delhi), Kalkaji, Govindpuri, New Delhi, 110019, India
[e] Department of Physics, Miranda House, University of Delhi, Delhi, 110007, India

ARTICLE INFO

Keywords:
MoS_2
Gas sensor
Transistor
Pulsed laser deposition
Schottky contact

ABSTRACT

Atomically thin layered semiconductors such as Molybdenum Sulphide (MoS_2) have emerged as potential candidate for trace level detection of chemicals owing to their innate very high surface to volume ratio. Present work focuses on the fabrication of room temperature operated Nitrogen dioxide (NO_2) gas sensor exploiting MoS_2 as gas sensing matrix. Three different sensor structures, (i) Au/Cr/single layer $MoS_2/Si_3N_4/Si$, (ii) Au/Cr/four-layer $MoS_2/Si_3N_4/Si$, and (iii) Au/Cr/ten-layer $MoS_2/Si_3N_4/Si$ were fabricated and gas sensing measurements were carried out for different NO_2 gas concentrations (1 ppm to 500 ppm). Effect of NO_2 gas adsorption on MoS_2 surface was explained using realignment of energy band diagram. Sensing response (%) for Au/Cr/four-layer $MoS_2/Si_3N_4/Si$ structure was found to be maximum as compared to the case of single layer and ten-layer structure and corresponding sensing mechanism has been investigated in detail. Response and recovery time of fabricated Au/Cr/four-layer $MoS_2/Si_3N_4/Si$ sensor were found to be 24 s and 41 s respectively, and cross selectivity measurements were performed and sensor was found to be highly selective towards NO_2 gas. Present work pave the way to realize the potential of MoS_2 based back gated Field Effect Transistors (FETs) for fabricating highly efficient NO_2 gas sensors.

1. Introduction

Gas sensing technology plays an important role in human and environmental security. The detection of toxic gases within a limited time frame is critical since its minor leakage can be extremely harmful to the living beings. There are several categories of materials which are conventionally used for the detection of these harmful/toxic gases such as metal oxides (thin and thick films) [1–4], nanorods [5–7], nanowires [8–10], conducting polymers [11–13] etc. Apart from that, in recent times, self-powered and wearable gas sensors are also becoming widely popular [14–18]. Metal-oxide based gas sensors have outperformed the other conventional materials due to their relative ease of fabrication making it a low-cost solution, good performance, ease of modification for enhancement of sensing performance, stability and industrial compatibility [19]. However, there are few issues with these metal-oxide based gas sensors: (i) their operating temperature is high (> 100 °C) which leads to a high power consumption [20], (ii) due to the high operating temperature there are undesired modification of grains in the matrix leading to the drift in performance [21], and (iii) they possess poor selectivity [22–24]. Conducting polymers are promising in this regard because they perform satisfactorily at room temperature (RT) but they are unstable and very sensitive to the humidity so that their device performance degrades in air and thus face problems with practical applications [25–27]. Recently 2D semiconducting materials such as MoS_2 has gathered lot of attention as sensors [28–31]. MoS_2 based FETs are extremely promising as gas sensing platform along with the advantage of

Abbreviations: MoS_2, molybdenum sulphide; NO_2, nitrogen dioxide; FETs, field effect transistors; RT, room temperature; DFT, density functional theory; LOD, limit of detection; HNPs, Hexagonal nanoplates; CNTs, Carbon nanotubes; PLD, Pulsed Laser Deposition; 2DSCs, Two-dimensional semiconductors; vdW, van der Waal; SR, Sensor Response.

* Corresponding author.
E-mail address: anjalisharma31@gmail.com (A. Sharma).

https://doi.org/10.1016/j.chphi.2025.100847
Received 28 December 2024; Received in revised form 4 February 2025; Accepted 7 February 2025
Available online 8 February 2025

Table 1
Deposition parameters for growing MoS_2 layers using PLD technique.

Process gas	N_2
Substrate Temperature	800 °C
Laser Fluence	0.8 J/cm^2
Growth pressure (Torr)	10^{-3}
Target to Substrate distance	6 cm
Numbers of Laser pulses	50, 150 and 400
Number of layers	1, 4 and 10

Table 2
Process parameter for deposition of metal electrodes on MoS_2 surface.

Electrode	Au/Cr
Deposition Technique	Thermal Evaporation
Source	Au/Cr wire
Filament current (A)	150/120 A
Growth pressure (Torr)	10^{-6}
Target Substrate distance (cm)	12
Deposition Time (min)	5

better electrostatic control to modulate the charge transfer process via MoS_2 due to interacting analyte. Density functional theory (DFT) suggests that MoS_2 surface have very good interaction coefficient for various hazardous gases like NO_2, SO_2, CO and NO etc. [32]. He et.al. fabricated flexible array of transistor utilizing MoS_2 as semiconducting channel and reduced graphene oxide as source-drain electrodes. They dispersed platinum (Pt) nanoparticles on the surface and achieved Limit of Detection (LOD) of 2 ppb with sensitivity of 6.1 % towards NO_2 gas [33]. Niu et.al. synthesized graphene/MoS_2 composite utilizing wet-spinning and hydrothermal method, and reported the LOD of 50 ppm towards NO_2 (sensitivity of 40 %) and 1000 ppm (sensitivity of 110 %) towards NH_3 gas respectively. rGO/MoS_2 composite based sensor showed sensitivity of 59.8 % towards 2 ppm NO_2 gas and achieved the LOD of 5.7 ppb at operating temperature of 60 °C [34]. Pham et al. demonstrated the role of incident photon with energy matching with band gap energy for enhancing the performance of MoS_2 based gas sensor [35]. They fabricated Au/Gr/MoS_2/Gr/Au/SiO_2/Si structure for sensing the NO_2 gas and achieved sensitivity of 3.3/ppb with LOD of 0.1 ppb for MoS_2 channel as sensing matrix. This concept paved the way for enhancing the interaction of 2D materials with analytes using the illumination of photon with energy equals to its band gap [35]. Wu et al. synthesized MoS_2/Si heterojunction where large area MoS_2 layers were synthesized by two step thermal decomposition process and Si nanowire (NW) array via chemical etching method [36]. Fabricated MoS_2/Si detected NO gas and reported the LOD to be 50 ppm with excellent repeatability and stability [36]. Park et.al demonstrated the advantage of dispersion of Pt nanoparticle on MoS_2, and achieved the LOD of 130 ppb and 5 ppm for NH_3 and H_2S gas respectively [37]. Wang et.al. demonstrated the interaction between MoS_2 and various gases using DFT and reported that CO (calculated adsorption energy is - 0.980 eV) and CH_4 (calculated adsorption energy is −0.710 eV) chemically adsorb on the MoS_2 surface whereas H_2 (calculated adsorption energy is −0.563 eV) follows the physical adsorption [38]. The fabricated Au-microsphere based sensor showed response of 25.48, 16.75, and 8.48 for 30 ppm of CO (operating temperature = 150 °C), CH_4 (operating temperature = 150 °C) and H_2 (operating temperature = 175 °C) respectively [38]. Deokar et.al. demonstrated unique coexistence of n-type and p-type region in synthesized hexagonal nanoplates (HNPs) over vertically grown carbon nanotubes (CNTs) using CVD technique [39]. They exploited the fabricated MoS_2 (HNPs)/CNT hybrid-based sensor for room temperature detection of NO_2 gas with LOD of 25 ppb. Their DFT calculation showed enhanced charge transfer at the comparably more active edge sites in HNPs MoS_2 [39]. Li et al. fabricated single and multilayer mechanically exfoliated MoS_2 based FET on SiO_2/Si substrates for sensing the NO gas at room temperature. The LOD of their sensor was 0.8 ppm and found that current stability of multilayer device is better than single layer device upon exposure of NO gas [40]. In summary, MoS_2 based sensors reported in literature are either having poor sensing response or working at relatively higher operating temperature. Apart from that, FET based sensors are scarcely reported. Thus, efforts have been made in the present work to resolve these issues by using pulsed laser deposition (PLD) grown MoS_2 layers.

Hence in the present work, an attempt has been made to fabricate highly sensitive room temperature (~27 °C) operated field effect transistor based NO_2 gas sensor using 2D-MoS_2 as gas sensing matrix. To explore the effect of gate modulation on the MoS_2 FET based sensor, three different configurations of sensor structure i.e. (i) Au/Cr/single layer MoS_2/Si_3N_4/Si, (ii) Au/Cr/four-layer MoS_2/Si_3N_4/Si and (iii) Au/Cr/ten-layer MoS_2/Si_3N_4/Si have been investigated in detail.

2. Experimental section

A 90 nm thin Si_3N_4 layer was grown on Si (n^{++}, resistivity: 0.001–0.005 Ω-cm) substrate using plasma enhanced chemical vapor deposition (PECVD) technique. Three different thicknesses of MoS_2 were explored, (i) single-layer (50 laser pulses at 800 °C substrate temperature), (ii) four-layer (150 laser pulses at 800 °C substrate temperature), and (iii) ten-layer (400 laser pulses at 800 °C substrate temperature) to see its effect on gas sensing performance. Different number of MoS_2 layers were grown using PLD technique and its optimization along with fabrication of FETs were reported in our previous work [41–43]. Since gas sensing is a surface dominating phenomenon, single-layer which have maximum possible surface to volume ratio and ten-layer MoS_2 (Bulk) having comparatively lesser surface to volume ratio were chosen. The gas sensors were fabricated by patterning the interdigitated electrode of gold (Au)/chrome (Cr) on MoS_2 layers using shadow mask. Process parameters involved in depositing the different MoS_2 layers are listed in Table 1. Au and Cr electrodes were deposited using pure metal (99.999 %) wire by thermal evaporation technique. The optimized process parameters for deposition of Au (50 nm)/Cr (50 nm) are listed in Table 2. Fig. 1 shows the schematic of the fabricated gas sensor using MoS_2 as gas sensing matrix, heavily doped Si as back gate and Au/Cr electrodes as source drain contacts. The three terminal electrical measurements for the fabricated MoS_2 based gas sensors with and without inclusion of gases were recorded using Keithley 4200 semiconductor characterization system which is integrated with probe station (Make: CASCADE Microtech, Germany).

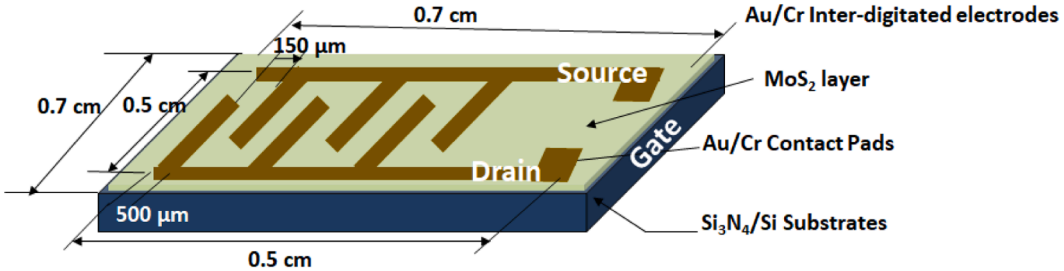

Fig. 1. Schematic of fabricated gas sensor for sensing NO_2 gas using MoS_2 layer as sensing matrix.

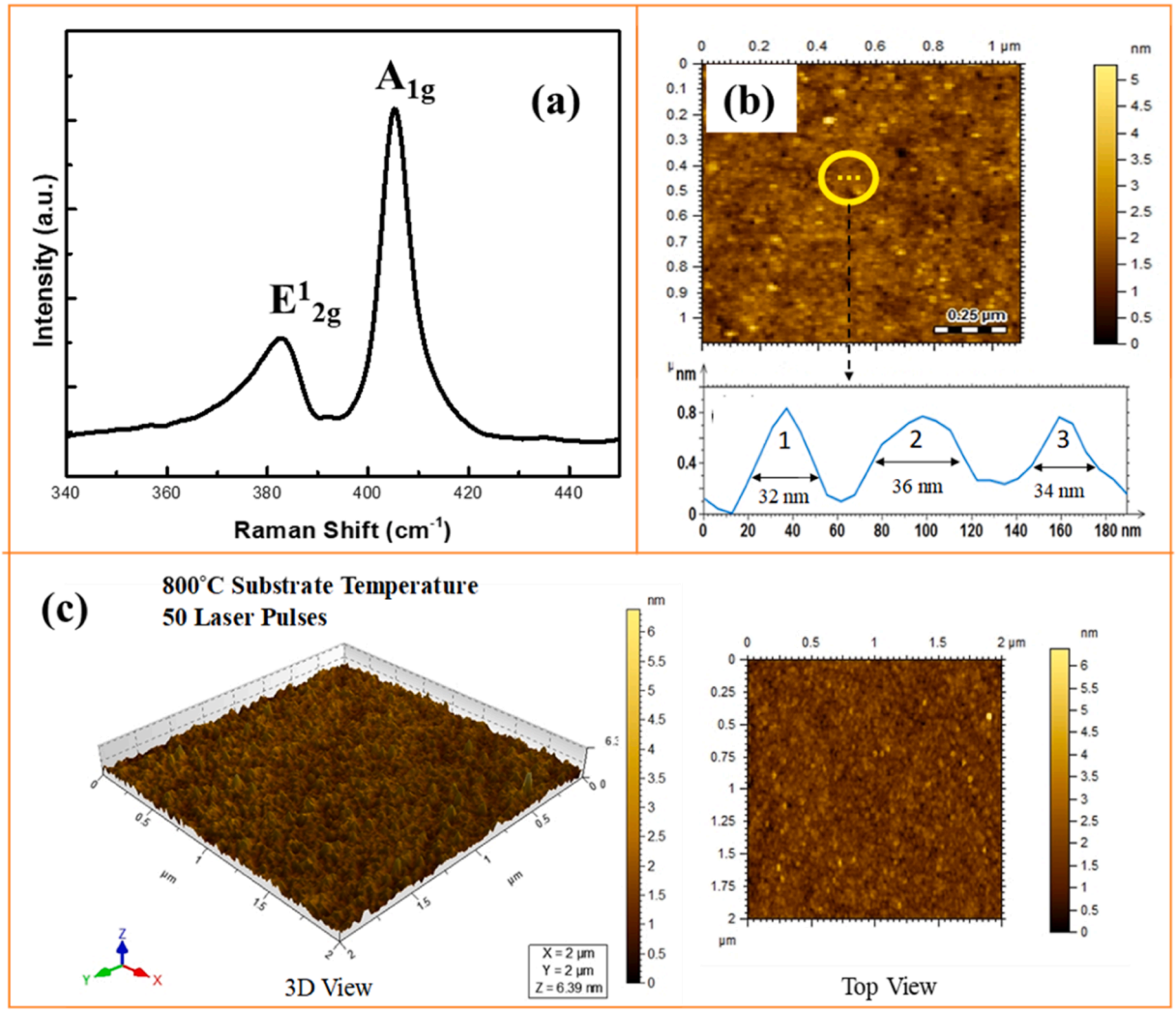

Fig. 2. Structural and surface morphologies studies of MoS_2 single layer: (a) Raman Spectra, AFM Profile (b) for 3 consecutive grains and (c) 3D view and top view of profile.

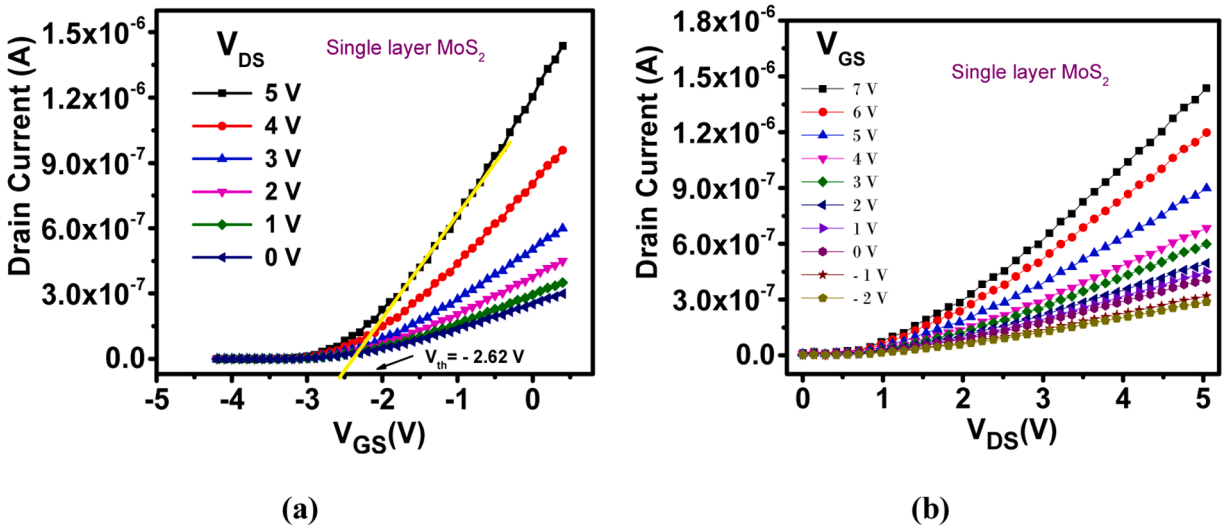

Fig. 3. (a) Transfer curve, and (b) output curve of the fabricated single layer MoS_2 FET.

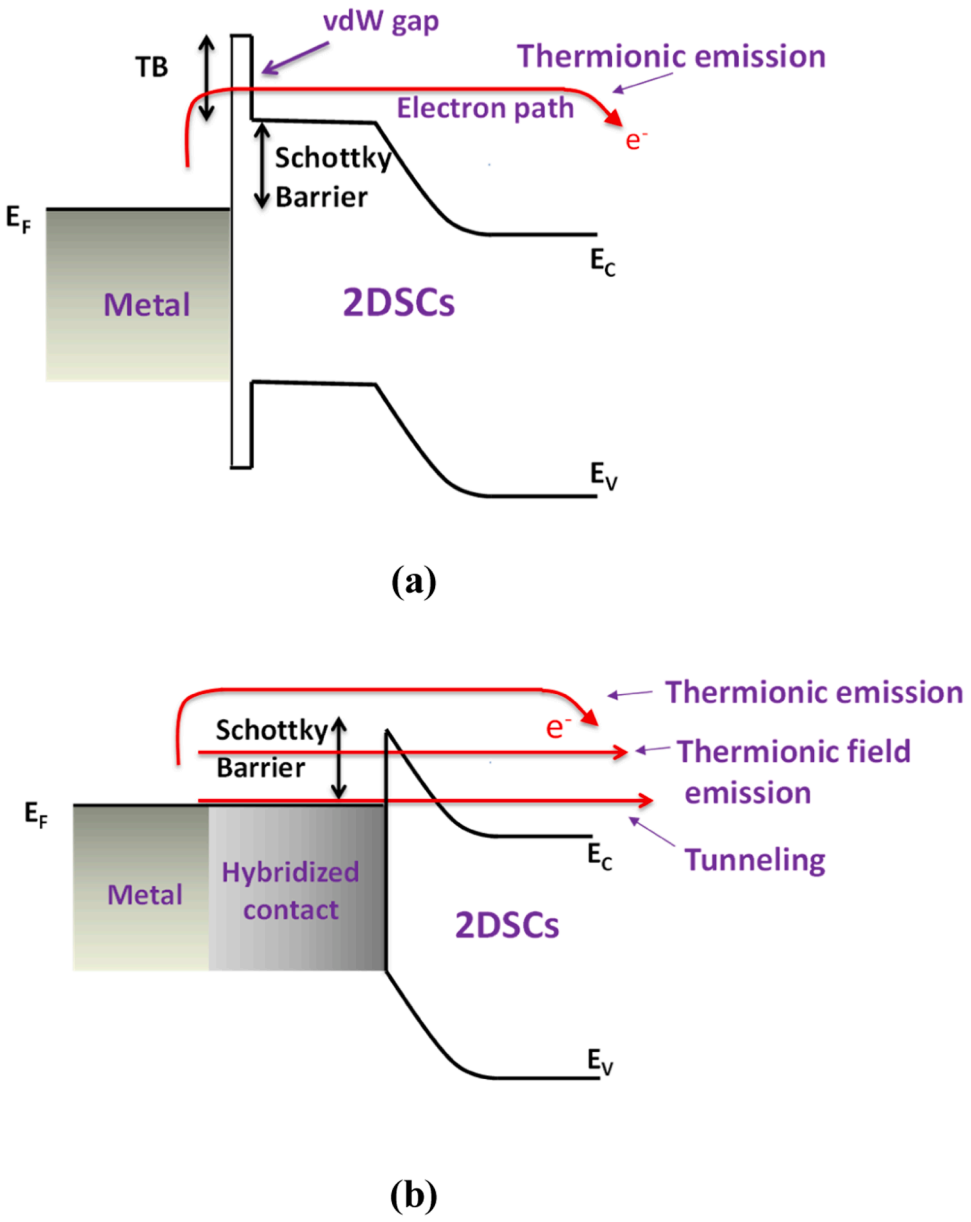

Fig. 4. Schematic of energy band diagram for (a) metal contact/2DSCs interface with van der Waal gap, and (b) metal contact/2DSCs interface with hybridization e.g., Chromium-MoS_2 interface.

3. Results and discussion

3.1. Characterization

Raman measurements of MoS_2 thin films grown using 50 laser pulses at substrate temperatures of 800 °C were carried out and the corresponding Raman spectra has been shown in Fig. 2(a). Peaks corresponding to $E^1_{2\,g}$ and $A_{1\,g}$ phonon modes were observed at 385.4 cm^{-1} and 405.2 cm^{-1} in the Raman spectrum respectively (Fig. 2(a)), confirming the growth of 2H-MoS_2 on passivated Si substrate. The wavenumber difference (directly correlated to the number of MoS_2 layers) between the two modes was estimated to be around $\Delta\omega \approx 19.8$ cm^{-1} for the prepared MoS_2 single layer. Fig. 2(b) show the 1×1 μm^2 scanned area of the sample grown with 50 laser pulses (monolayer), along with the corresponding grain size distribution profile. Three consecutive grains of the sample were profiled and corresponding distribution shows non-uniform distribution of the three consecutive grains (32 nm, 36 nm and 34 nm) suggesting inhomogeneous growth of MoS_2 monolayer by PLD at 800 °C using 50 laser pulses. Fig. 2(c) shows the 3D and top view micro-images of the MoS_2 monolayers grown at substrate temperature of 800 °C with 50 laser pulses. Scanning area of the samples was fixed at 2×2 μm^2. The step coverage of the sample grown at 800 °C is continuous (Fig. 2(c)) indicating the growth of high quality MoS_2 layers, which is in accordance with the results obtained using Raman spectroscopy for sample grown with 50 laser pulses.

3.2. Gas sensing using single layer MoS_2 as gas sensing matrix

MoS_2 possess very high surface to volume ratio specially in their single layer form. Gas sensing is surface dominating phenomenon and thus atomically thin layered material is expected to offer high detection capability for the incident chemical species. For the semiconducting materials, their conductance plays an important role in the detection capability which can be effectively tuned using gate terminal of FET. MoS_2 is an atomically thin layered semiconductor which gives extra degree of freedom to modulate its conductance using back-gate. By

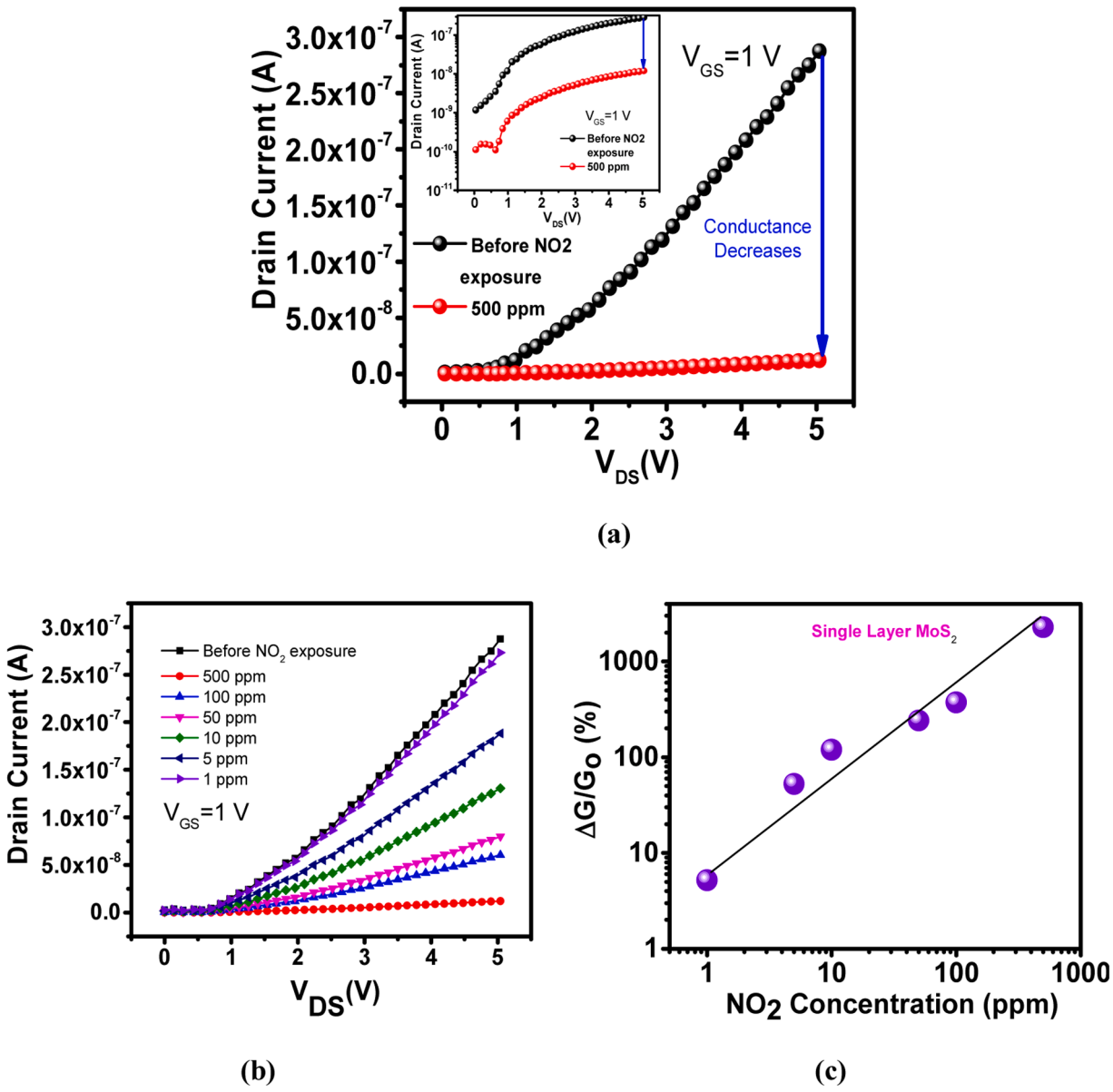

Fig. 5. Output curve for single layer MoS_2 FET sensor at $V_{GS} = 1$ V without and with exposure towards (a) 500 ppm NO_2 gas, and (b) towards different concentration (1 ppm to 500 ppm) of NO_2, and (c) sensor response variation with concentration of NO_2 gas on logarithmic scale.

effective modulation from back-gate, one can manipulate the properties of the active matrix to enhance its sensing functionalities [44]. It may be noticed that, "back-gate" geometry of FETs is extremely useful for gas sensing applications as it can provide both, (i) effective interaction area of sensing matrix for target gas species, and (ii) necessary modulation of channel conductance from back-gate. Fig. 3(a) and (b) show the transfer and output characteristic curves for the fabricated back-gated FET using MoS_2 as semiconducting channel respectively. It can be observed from Fig. 3(a) that fabricated transistor shows n-type behavior of semiconducting MoS_2 with a threshold voltage of −2.62 V. The mobility of the fabricated device using single layer MoS_2 was estimated to be 21.5 $cm^2V^{-1}S^{-1}$ with $I_{on/off}$ ratio 3.4×10^4. The shape observed in output curve (Fig. 3(b)) for MoS_2 devices originates from the existence of Schottky barrier at MoS_2 and Cr interface and these kind of devices are proven to be more advantageous for sensing study related to gas-solid interactions [45]. Since monolayer MoS_2 possess high surface area and top side of its surface is open to ambient, charge transport is expected to be very sensitive to the interaction with target gas molecules.

In contrast with the metal contact with three-dimensional semiconductors, pristine surface of two-dimensional semiconductors (2DSCs) avoid forming covalent bonds with many metals in top-contact configuration [45]. If there is no hybridization between 2DSCs and metal contact, there exist additional van der Waal (vdW) gap (tunnel barrier) between the two. This existence of vdW greatly reduces the carrier injection compared to the case when there is no vdW gap (only inherent Schottky barrier is there [45]. The former case is seen in MoS_2 with metal contacts like Gold (Au) while the presence of metal like Cr forbids the formation of vdW gap and only an inherent Schottky barrier is formed [45]. Cr with MoS_2 gives rise to the formation of a hybrid contact due to formation of bonds between metal and 2DSCs [45–47]. Fig. 4(a) and (b) show the schematic of energy band diagram to understand this better. A tunnel barrier (TB) is formed due to vdW gap between gold with 2DSCs as shown in Fig. 4(a) restricting the flow of charge carriers. In this case electron flow from metal to semiconductor is possible only through thermionic emission [45]. On the other hand, use of metals like Cr with 2DSCs materials is reported to form a hybridized contact with 2DSCs avoiding the formation of TB (Fig. 4(b)). The presence of this hybridized contact facilitates the flow of charge carriers

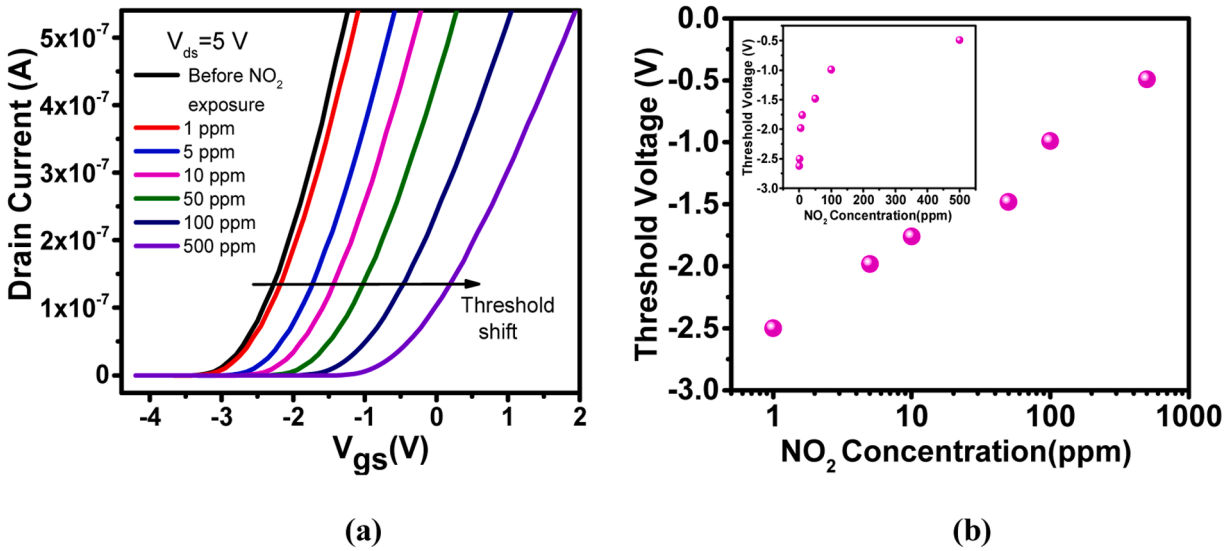

Fig. 6. (a) Transfer curve at V_{DS} = 5 V of single layer MoS_2 FET sensor towards NO_2 gas from 1 ppm to 500 ppm, and (b) threshold voltage variation with gas concentration on logarithmic scale and inset shows the same variation on linear scale.

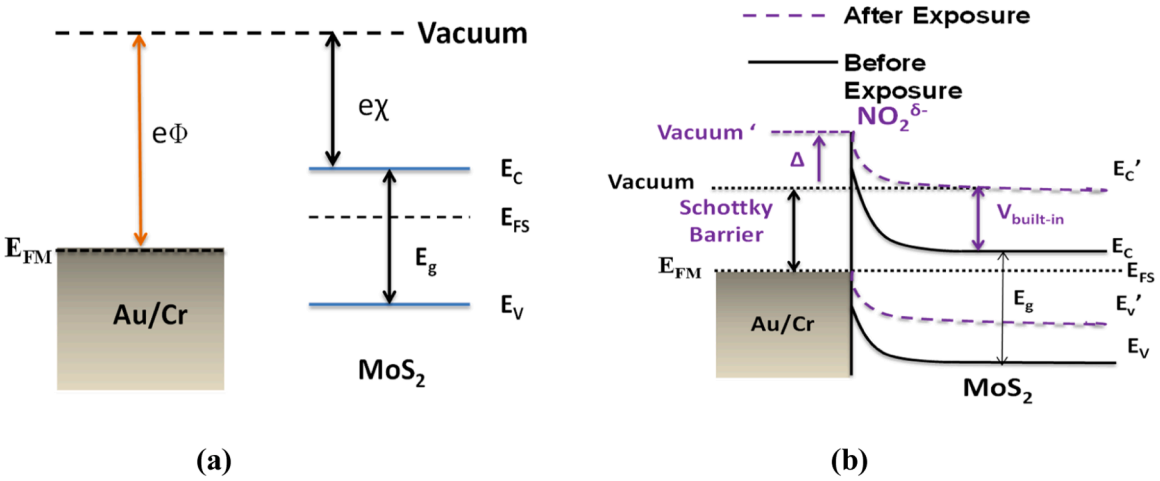

Fig. 7. (a) Schematic of energy band of Au/Cr metal system and single layer MoS_2 in isolated state and under thermal equilibrium, and (b) band realignment and energy diagram of MoS_2 and Au/Cr after Schottky barrier formation and dashed purple line show the change in energy band after NO_2 exposure.

across the metal/2DSC interface through, (i) thermionic emission, (ii) thermionic field emission, and (iii) tunneling. The results are well established by Allain et.al. theoretically using DFT simulations as well as experimentally [45]. Based on this background, Au/Cr bilayer metal contact was used in the present work to provide a hybridized Schottky contact with MoS_2.

NO_2 being hazardous and toxic gas has been chosen as the target gas to study the conductance variation offered by single layer MoS_2 and its behavior with channel modulation in back gate configuration. Fig. 5(a) shows the output curve of single layer MoS_2 FET at V_{GS} = 1 V obtained under before and after the 500 ppm exposure of NO_2 gas with Zero Grade Air (ZGA) (80 % N_2 + 20 % O_2) as the carrier gas at room temperature (~27 °C). The value of gate voltage is chosen such that device is in the "ON" state and any slight change in channel conductance can be observed. There is significant decrease in conductance of FET when 500 ppm NO_2 gas was exposed on the surface of single layer MoS_2 (Fig. 5(a)) over the entire measure range of V_{DS}. The observed decrease in conductance is attributed to the oxidizing nature of NO_2 gas. It was also observed that with further increase in gate voltage only the drain current value increases while change in conductance remains constant because device is already in ON state. Since NO_2 is an oxidizing gas which accept electrons from MoS_2, it reduces the number of charge carrier participating in the drain current, thereby reducing the I_{DS} (Fig. 5(a)) and hence lower the channel conductance. Apart from the NO_2, the MoS_2 can also interact with the ambient oxygen to form O_2^- or O^- ions (Eqs. (1) and (2)) So, the NO_2 molecules can either interact directly with MoS_2(Eq. (3)) or through these oxygen ions (Eqs. (4) and (5)) leading to a change in the resistance [48].

$$O_2 + e^- \rightarrow O_2^- \quad (1)$$

$$O_2 + 2e^- \rightarrow 2O^- \quad (2)$$

$$NO_2(gas) + e^- \leftrightarrow NO_2^-(ads) \quad (3)$$

$$NO_2(gas) + O_2^-(ads) + 2e^- \rightarrow NO_2^-(ads) + 2O^-(ads) \quad (4)$$

$$NO_2(gas) + O^-(ads) + 2e^- \rightarrow NO_2^-(ads) + 2O_2^-(ads) \quad (5)$$

After the observance of significant decrease in conductance for 500 ppm NO_2 exposure, a systematic variation in NO_2 gas concentration (1 ppm to 500 ppm) was carried out as shown in Fig. 5(b). It may be noticed from Fig. 5(b) that there is systematic change in the conductance with

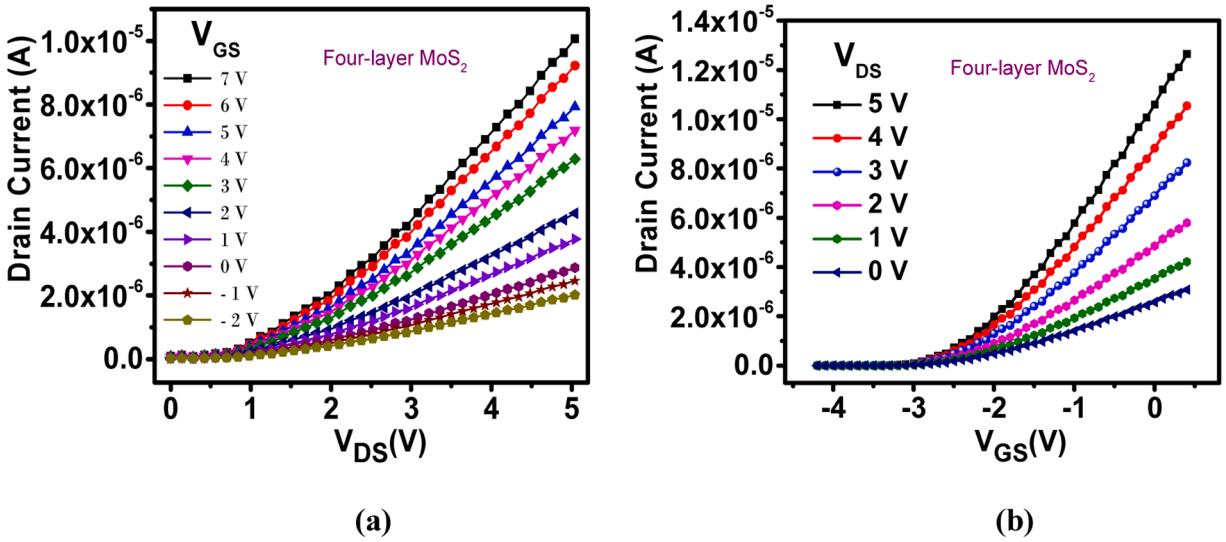

Fig. 8. (a) Output curves and (b) transfer curves of the fabricated four-layer MoS_2 channel-based FET devices.

increase in concentration of gas tested from 1 ppm to 500 ppm, showing high sensitivity of the fabricated sensor towards NO_2 gas. The sensitivity of the fabricated sensor can be estimated by quantifying the conductance change corresponding to each gas concentration. Sensor response (SR) can be defined as percentage change in the conductance value of the FET with and without gas exposure. If G_0 is the channel conductance before the gas exposure and G_S is the conductance after the gas exposure, mathematically,

$$SR = \frac{G_o - G_s}{G_s} \times 100\% \tag{6}$$

where, $\Delta G = G_0 - G_s$ is the change in channel conductance with exposure to target gas. Fig. 4(c) shows the graph for SR with different concentration of NO_2 gas exposed to single layer MoS_2 FET on logarithmic scale. The SR (%) sensor was found to be 5.2, 52.8, 120, 242, 375 and 2280 towards 1, 5, 10, 50, 100 and 500 ppm concentration of NO_2 gas respectively. It can be noticed from Fig. 5(c) that there is linear variation of SR on log-log scale justifying the robust behavior of fabricated sensor.

To understand the mechanism of NO_2–MoS_2 interaction and its aftermaths on the sensor response (SR), transfer curves were obtained for different concentration of gas. Fig. 6(a) shows the transfer curve of single layer MoS_2 FET without and with exposure to different concentration of NO_2 gas. Fig. 6(b) shows the change in threshold voltage with exposed gas concentration on logarithmic scale and inset shows the corresponding change on the linear scale. A monotonic increase in threshold voltage (V_{th}) towards positive gate voltage is observed with increasing the concentration of NO_2 gas (Fig. 6(b)). This positive shift in the V_{th} suggests that understanding about the change in the channel conductance with NO_2 interaction is crucial to identify the sensing mechanism of MoS_2 FET sensor. The total resistance (R_{total}) of the single layer MoS_2 FET is the sum of resistance offered by MoS_2 layer (R_{MoS2}) and contact resistance ($R_{contact}$) that exists at metal contact (Au/Cr) and MoS_2 interface, i.e.

$$R_{total} = R_{MoS2} + R_{contact} \tag{7}$$

It is well known that resistance of the semiconducting materials (MoS_2) is inversely dependent on carrier concentration (N_c), mathematically [49]

$$R_{semiconductor} \; \alpha \; \frac{1}{N_c} \tag{8}$$

But contact resistance ($R_{contact}$) is dependent on carrier concentration (N_c) as well as the height of Schottky barrier (φ) that exists at the Au/Cr and MoS_2 interface, i.e.

$$R_{contact} \; \alpha \; \frac{1}{N_c} e^{(\varphi / k_b T)} \tag{9}$$

Where k_b is Boltzmann's constant and T is the ambient temperature. Hence, any change in the electron concentration or Schottky barrier height will result in the change in conductance of the single layer MoS_2 FET. In the present case, there is charge transfer between NO_2 gas molecules and MoS_2 surface because NO_2 has one lone pair electron which tends to extract one electron from MoS_2 conduction band to make itself stable [50]. This way NO_2 acts as strong oxidizing agent and reduces the concentration of electron in conduction band of MoS_2, thereby reducing the channel conductance with NO_2 interaction. Thus, after exposure to NO_2 gas, it requires more positive voltage at gate terminal to turn ON the fabricated transistor [33]. It is obvious that more concentration of NO_2 will reduce more electrons from conduction band of MoS_2 and thus more and more positive gate voltage is required for switching ON the transistor which can be clearly seen in Fig. 6(a) and (b). Further, the total conductance of the device is affected by the change in Schottky barrier height (Eqs. (7) and (9)).

Fig. 7(a) shows the schematic of energy band diagram corresponding to Au/Cr metal system and single layer MoS_2 in isolate state and under thermal equilibrium condition. E_{FS}, E_c, and E_v in Fig. 7(a) represent the Fermi energy level, bottom of conduction band, top of valence band of single layer MoS_2 respectively, whereas, symbols E_{FM}, Φ represent the Fermi energy level and work function of metal (Cr) respectively, and χ represents the electron affinity of single layer MoS_2 ($\chi = 4.5$ eV). In the isolated state, fermi level of chromium (E_{FM}) lies between the bottom of conduction band (E_c) and top of valence band (E_v) of single layer MoS_2 (Fig. 7(a)). Fig. 7(b) shows the schematic of energy band diagram when Au/Cr metal electrodes makes Schottky barrier with single layer MoS_2 under thermal equilibrium and modification in Schottky barrier (height and width) upon absorption of NO_2 gas. Since the deposited Au/Cr is making top contact with MoS_2 layer, work function of chromium ($\Phi = 4.5$) is considered in Fig. 7(b). When chromium is in contact with MoS_2 layer, band bending of MoS_2 takes place to align the fermi levels and there exist a Schottky barrier with height:

$$\varphi(\text{eV}) = \Phi(\text{chromium}) - \chi(\text{single layer } MoS_2) \tag{10}$$

As discussed earlier, on exposure of the sensor device with NO_2 gas, conductance change of the device is dependent on majorly two phenomena, (i) transfer of charge from MoS_2 to NO_2 gas, and (ii) change in Schottky barrier upon gas exposure. The width of the Schottky barrier

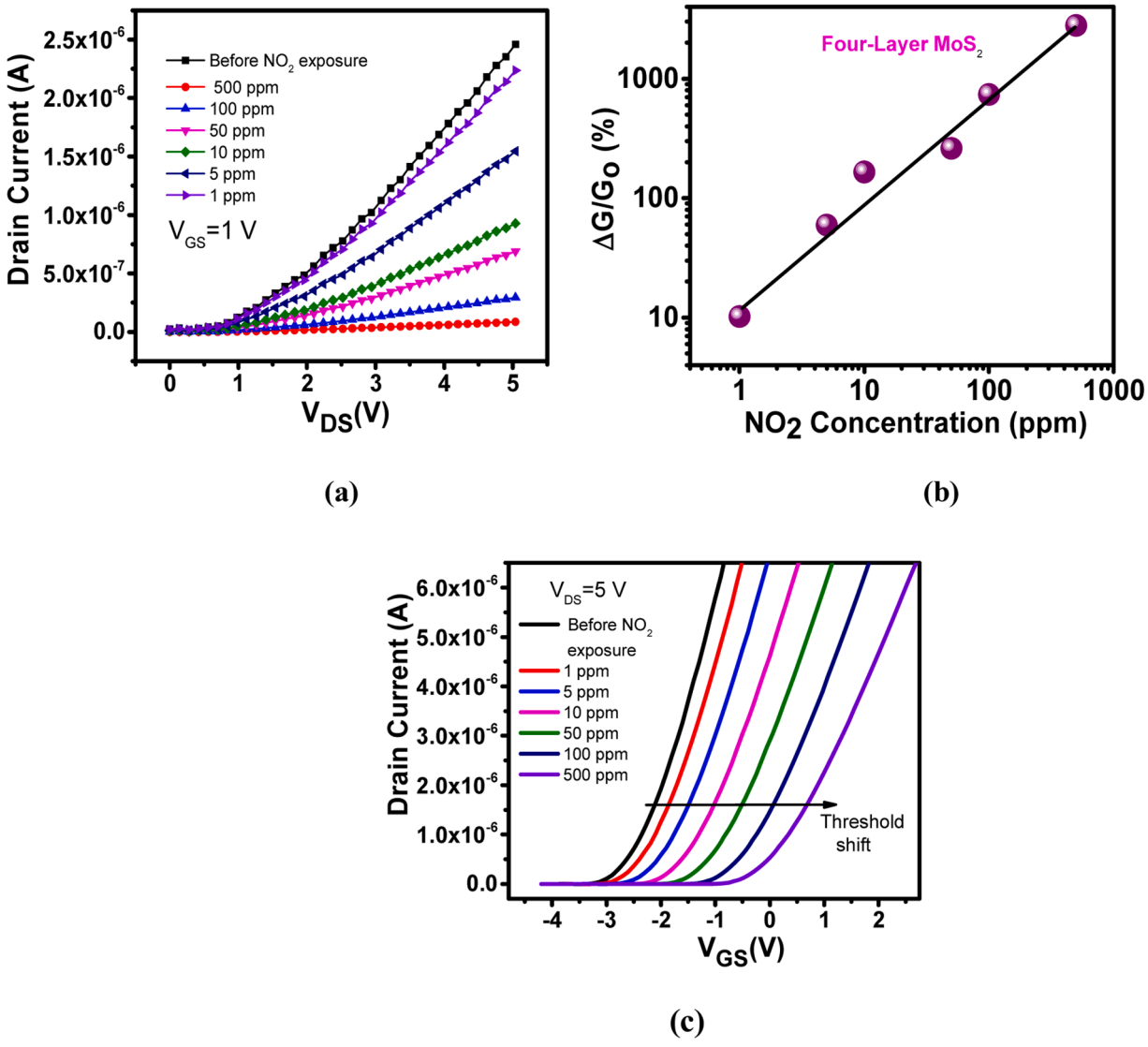

Fig. 9. (a) Output curve for four-layer MoS_2 FET sensor without NO_2 exposure and exposure to different concentration of NO_2 from 1 ppm to 500 ppm, (b) four-layer MoS_2 FET sensor response variation with concentration of NO_2 gas on logarithmic scale, and(c) transfer curve at $V_{DS} = 5$ V of fabricated four-layer MoS_2 FET sensor towards NO_2 gas from 1 ppm to 500 ppm gas concentration.

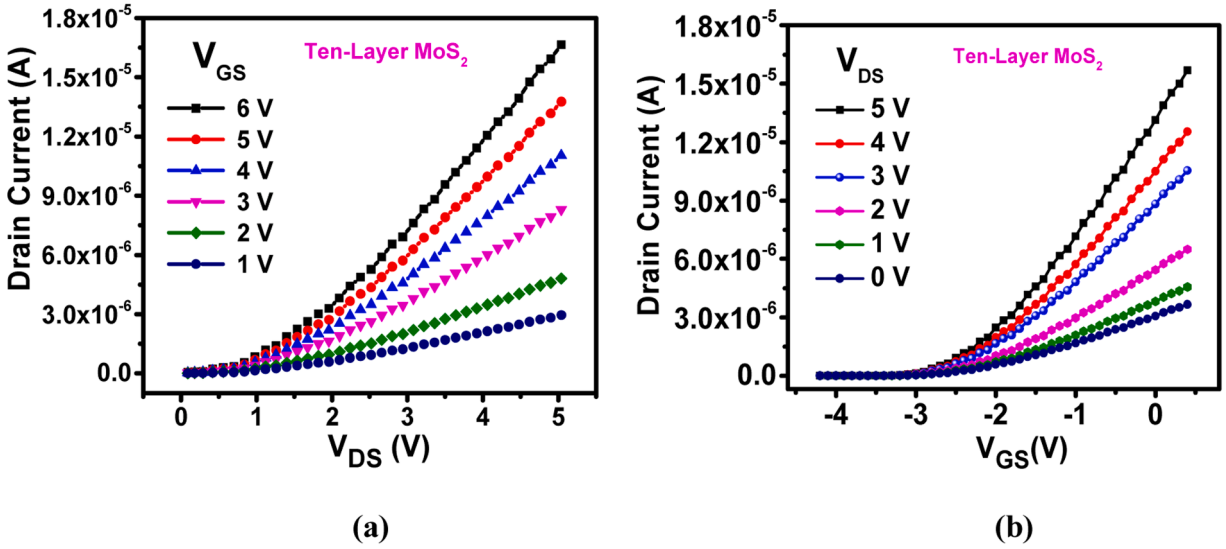

Fig. 10. (a) Output curves, and (b) transfer curve of the fabricated ten-layer MoS_2 channel-based FET device.

will increase and built-in potential ($V_{built\text{-}in}$) will modify when absorption of NO_2 gas takes place (Fig. 7(b)). With reduction in electron concentration in conduction band of MoS_2 upon absorption of NO_2 gas, fermi level of MoS_2 will move downwards. This downward movement of fermi level will result in increment in Schottky barrier width and reduces $V_{built\text{-}in}$, resulting in overall decrement in current in the device (Fig. 7 (b)) [51–53]. NO_2 withdraw electrons from the MoS_2 and become $NO_2^{\delta-}$ (negatively charged species) which increases the height of Schottky barrier (Δ) as shown in Fig. 7(b). This kind of increase is commonly found in literature, e.g. oxygen in oxidative state increases the Schottky barrier height of ZnO nanowires and created profound effect in performance of ZnO nanowire transistor [54]. Hence, upon exposure of NO_2 gas, conductance of the single layer MoS_2 FET decreases due to both modification in Schottky barrier and transfer of charge phenomenon.

3.3. Gas sensing using four-layer and ten-layer MoS_2 as sensing matrix

Gas sensing is a surface-controlled process. It is to understand that only certain thickness i.e. 80 nm to 100 nm of sensing matrix (especially in oxide) semiconductors such as Tin oxide (SnO_2), Zinc oxide (ZnO) etc. participates in the interaction with analytes [55]. When adsorption of gas takes place, fix depth of electron depletion layer of thickness range 2–100 nm is formed [21]. This depth is called Debye length (L) which is defined as the distance over which maximum charge separation can takes place. When crystallite size (D) is smaller than 2 L, each grain is depleted of conducting electrons and the resistance offered by the grains control the sensing response and mechanism is called grain control [21]. To identify the optimum thickness of MoS_2, four-layer and ten-layer MoS_2 as gas sensing matrix was also investigated in the present work. Fig. 8(a) and (b) show the output and transfer curves for the MoS_2 FET fabricated using four-layer MoS_2 as channel layer. Fig. 8(a) again shows the expected Schottky contact formation of Cr with MoS_2 layers. It can be noticed from Fig. 8(b) that drain current values has increased from 1.45×10^{-6} A (case of single layer MoS_2 sensor) to 1.28×10^{-5} A at V_{DS} = 5 V and V_{GS} = 1 V for four-layer MoS_2 device. This increase in the drain current is likely due to increased density of states (number of electrons) for the case of four-layer MoS_2 compared to single-layer MoS_2 [56]. The fabricated transistor shows expected n-type behavior of semiconducting MoS_2 with a threshold voltage of −2.62 V (Fig. 8(b)). The mobility of the device using four-layer MoS_2 was estimated to be 26.8 $cm^2V^{-1}S^{-1}$ with current on/off ratio of 4.2×10^5. The mobility and current on/off ratio both increases for the case of four-layer MoS_2 FET compared to the corresponding value obtained for single layer MoS_2 based FET.

To check the gas sensing behavior of four-layer MoS_2 FET, different concentrations of 1, 5, 10, 50, 100 and 500 ppm of NO_2 gas was exposed separately in gas testing chamber. Fig. 9(a) shows the output curves of FET sensor obtained at V_{GS} = 1 V when sensor was exposed to different gas concentrations. As expected, drain current is seen to be continuously decreasing with increasing the NO_2 gas concentration at a fixed value of V_{GS} and all measured values of V_{DS}. Variation of Sensor Response (SR) with NO_2 gas concentration on logarithmic scale is shown in Fig. 9(b). The SR (%) sensor was found to be 10.2, 59.4, 165.3, 261.1, 737 and 2790 towards 1, 5, 10, 50, 100 and 500 ppm concentration of NO_2 gas respectively. It can be noticed from Fig. 9(b) that there is linear variation of SR on log-log scale as observed for the case of single layer, justifying the robust behavior. Fig. 9(c) shows the transfer curve obtained for the four-layer MoS_2 FET without and with exposure to different concentration of NO_2 gas. A monotonic increase in threshold voltage (V_{th}) towards positive gate voltage is observed with increasing the concentration of NO_2 gas (Fig. 9(c)). This increment is consistent with results obtained for single layer MoS_2 FET based sensor (Fig. 6(a)).

Fig. 10(a) and (b) show the output curves and transfer curves obtained for ten-layer MoS_2 FET device respectively.

To observe the gas sensing response, different concentration of NO_2 gas from 500 to 1 ppm was introduced systematically into the test chamber separately and its effect on the transfer and output curves were recorded as shown in Fig. 11(a) and (b) where inset of Fig. 10(a) shows the variation on semi-log scale. A slight change in the drain current was observed with a SR of 16.2 % towards 500 ppm NO_2 gas (Fig. 11(a)). However, SR was reduced for the lower concentrations (SR of 9.1 % for 100 ppm, SR of 6 % for 50 ppm, SR of 3.7 % for 10 ppm, SR of 2.06 % for 5 ppm and SR of 1.71 % for 1 ppm) which is lower than the corresponding values obtained for devices using single layer (Fig. 5(c)) and

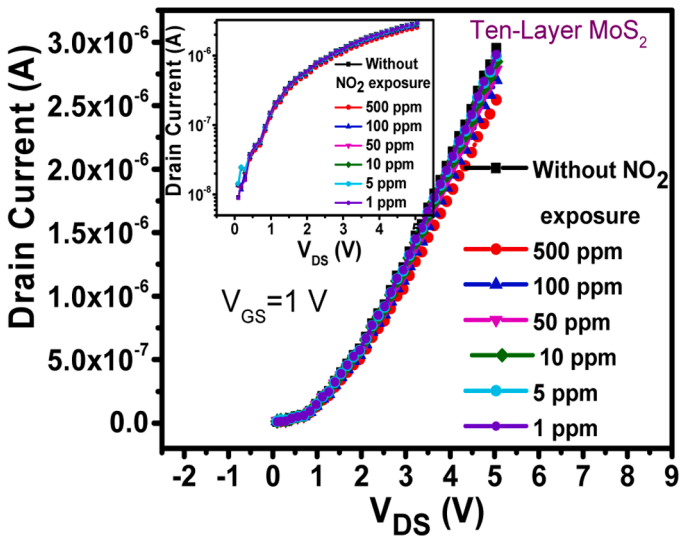

(a)

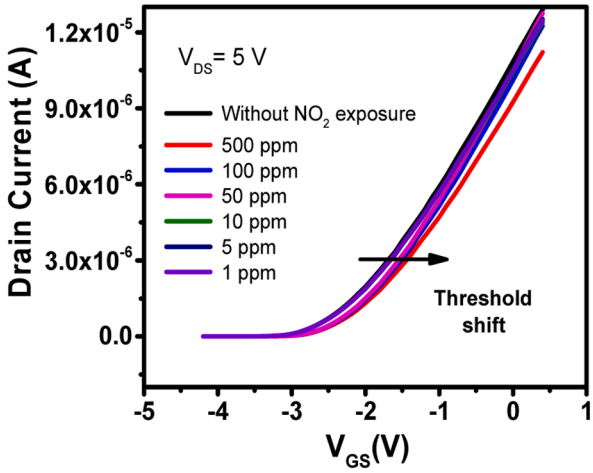

(b)

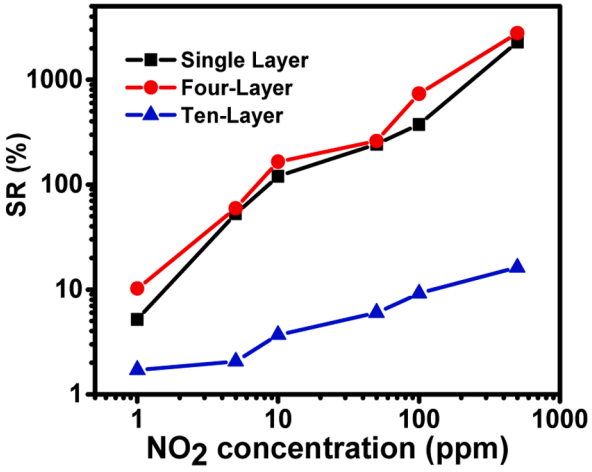

(c)

Fig. 11. (a) Output curve for ten-layer MoS_2 sensor (inset shows the variation on semi-log scale), (b) transfer curves obtained for ten-layer MoS_2 FET sensor without NO_2 exposure and exposure to different concentration of NO_2 from 1 ppm to 500 ppm, and (c) comparison of sensing response between single layer, four-layer and ten-layer MoS_2 FET sensors with concentration of NO_2 gas.

Table 3
Values of conductance in absence and presence of 10 ppm NO_2 gas and sensing response for single layer, four layer and ten-layer MoS_2 based FET structures.

No. of MoS_2 layers	G_0 (Siemens)	G_s (Siemens)	SR (%)
Single	4.39×10^{-8}	2.0×10^{-8}	120
Four	3.76×10^{-7}	1.42×10^{-7}	165.3
Ten	4.51×10^{-7}	4.35×10^{-7}	3.69

four-layer MoS_2 (Fig. 9(b)) channel. The obtained results signify the lesser sensitivity of the fabricated device with ten-layer MoS_2 as sensing matrix. Transfer curve of ten-layer MoS_2 was also traced for the exposure of 500 ppm to 1 ppm NO_2 gas concentration (Fig. 11(b)). There was slight change in the threshold voltage on exposure of 500 ppm gas, however a negligible change was observed for lower concentrations (100 ppm to 1 ppm) as expected from the SR observed in the output characteristics. Fig. 11(c) shows the graph of SR (%) with concentrations of NO_2 gas for FET sensors having single layer, four-layer and ten-layer MoS_2 channels for comparison. It can be noticed from Fig. 11(c) that SR

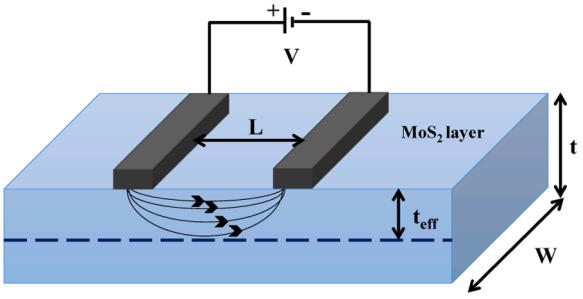

Fig. 12. Schematic of sensing structure showing electric field profile for effective thickness upto which maximum interaction is possible.

(%) is maximum for the FET sensor having four-layer MoS_2 compared to single layer and ten-layer MoS_2 sensors for each NO_2 concentration. It is concluded that MoS_2 sensor with four-layer MoS_2 as sensing matrix is optimum for the high performance NO_2 gas sensor.

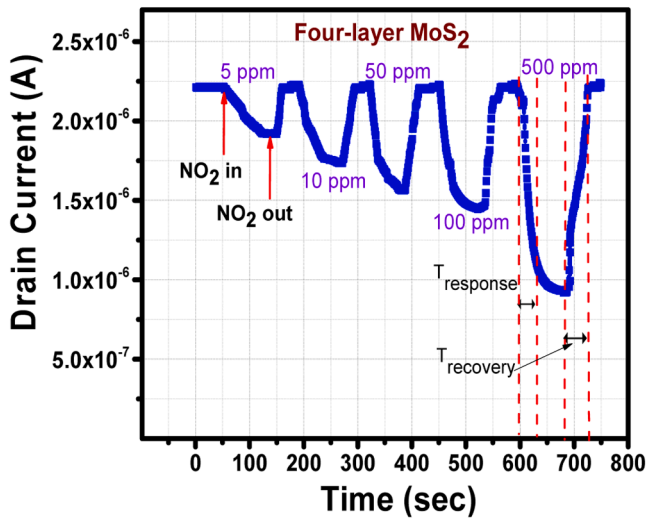

(a)

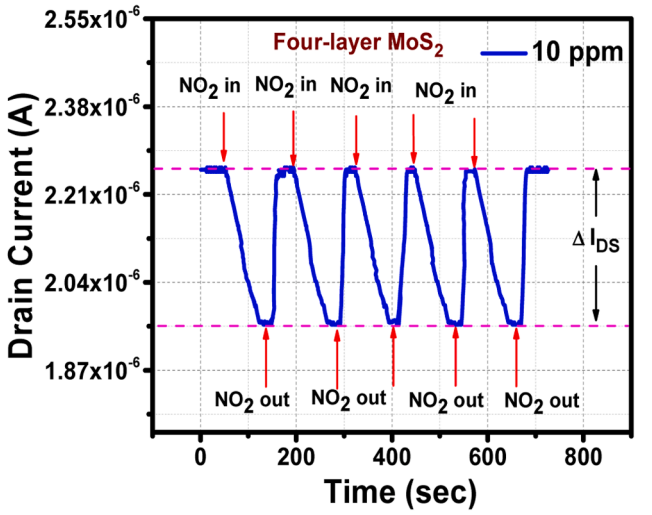

(b)

Fig. 13. Transient response of 4 layers MoS_2 FET sensor (a) towards different concentration of NO_2 gas, and (b) towards 10 ppm of NO_2 gas with 5 repeated cycles.

3.4. Explanation of higher sensitivity achieved for four-layer MoS_2 FET sensor

The higher sensing response of four-layer MoS_2 based FET structure as compared to single layer and ten-layer MoS_2 structure can be well understood in terms of conductance change with number of MoS_2 layers upon interaction with NO_2 gas. Table 3 summarizes the value of conductance in presence (G_S) and absence (G_0) of 10 ppm of NO_2 gas. The value of conductance is found to be, $G_0 = 4.39 \times 10^{-8}$ S and $G_S = 2.0 \times 10^{-8}$ S for single layer, $G_0 = 3.76 \times 10^{-7}$ S and $G_S = 1.42 \times 10^{-7}$ four-layer and $G_0 = 4.51 \times 10^{-7}$ S and $G_S = 4.35 \times 10^{-7}$ for ten-layer MoS_2 FET structure respectively towards 10 ppm of NO_2 gas. The conductance ($G = 1/R$) of a FET structure having MoS_2 sensing layer can be expressed as a function of film thickness as

$$G = \frac{1}{R_a} = \frac{A\sigma}{L} = \frac{Wt\sigma}{L} \tag{11}$$

where, σ is electrical conductivity and t is the thickness of MoS_2 layer, and L and W are the distance between two electrodes and length of electrodes respectively as shown in Fig. 11. The Eq. (11) is valid for the FET structure having MoS_2 layer of thickness over the range $t = 0$ to t_{eff}, where t_{eff} is the effective thickness of sensing layer upto which applied electric field is confined (Fig. 12) i.e. about four layer. If $t > t_{eff}$, $G = \left(\frac{W\sigma}{L}\right) t_{eff}$, and G of prepared sensor must show a lesser sensitivity beyond a certain thickness if there is lesser availability of electrons to interact with incoming analyte. Since, gas sensing is a surface dominating phenomenon, it limits the number of gas molecules to get chemically adsorbed on the surface of the sensing matrix. NO_2 gas molecules can easily get diffused on the surface of MoS_2 upto a certain thickness (space-charge layer). This diffusion on MoS_2 surface for the case of four-layer MoS_2, increases the probability of charge transfer process since electron from all the four-layer MoS_2 channel can participate and hence maximum probability of decrement in the conductance is expected resulting in great improvement in SR [50]. While, for the case of single layer MoS_2, NO_2 gas molecules does not have any access to go deep so lesser amount of diffusion can take place resulting in lesser quantity of adsorption which in turn leads to comparably lesser probability of charge transfer between MoS_2 and NO_2. This lesser charge transfer means lesser change in conductance hence lower sensitivity for the case of single layer MoS_2. There is a very small change in the conductance value on exposure to gas in ten-layer MoS_2 FET structure leading to poor sensing performance. This may be attributed to the fact that on further increasing the number of layers (more than four layers), there is saturation in effective thickness (t_{eff}) of the sensing matrix as well as the increased interlayer resistance (due to increment in vdW gap) limits the number of electron (due to loss of gate electrostatic control with increased thickness) to participate in the interaction with incoming NO_2 gas, resulting in the poor sensing response of bulk MoS_2. However, for the case of four-layer MoS_2 sensor, there is effective gate electrostatic control such that electron from all the four layers can participate in the space charge formation resulting in very high probability of electron transfer, thus higher sensing response. Thus, four-layer MoS_2 is identified as the effective thickness give maximum change in the value of conductance and hence higher sensing response.

3.5. Response time of four-layer MoS_2 FET sensor

Fig. 13(a) shows the transient response (variation in drain current with time) of the prepared four-layer MoS_2 based device as a function of time for different concentrations of NO_2 gas ranging from 5 ppm to 500 ppm. The drain current values are found to be decreasing from 2.26×10^{-6} A (without NO_2 exposure) to 1.89×10^{-6} A (5 ppm NO_2) gas, 1.74×10^{-6} A (10 ppm NO_2), 1.56×10^{-6} A (50 ppm NO_2), 1.44×10^{-6} A (100 ppm) and 9.2×10^{-7} A (500 ppm NO_2) gas (Fig. 12(a)). The response time of the FET sensor can be defined as time required for the 90 % change in the conductance value at a particular gas concentration. The response ($T_{response}$) and recovery time ($T_{recovery}$) of fabricated four-layer MoS_2 channel based device is found to be 24 s and 41 s respectively (Fig. 13(a)). This response time at room temperature is comparable to the recent reported values for conducting polymers and carbon nanotubes and also to MoS_2 based gas sensors [40,57,58,59]. Fig. 13(b) shows the transient response of fabricated four-layer MoS_2 device towards 10 ppm NO_2 gas with 5 repeated cycle to identify the repeatability and reproducibility. The fabricated sensor exhibits similar response characteristics for each cycle without showing any drift in the drain current values (Fig. 13(b)). The obtained result suggests that fabricated four-layer device is highly stable and repeatable towards NO_2 gas.

3.6. Cross-selectivity studies of four-layer MoS_2 FET sensor

The fabricated four-layer MoS_2 FET sensor was tested for cross-selectivity with different interfering gases. Fig. 14(a) shows the response (I_{DS}-V_{DS}) curve of four-layer MoS_2 based FET sensor recorded

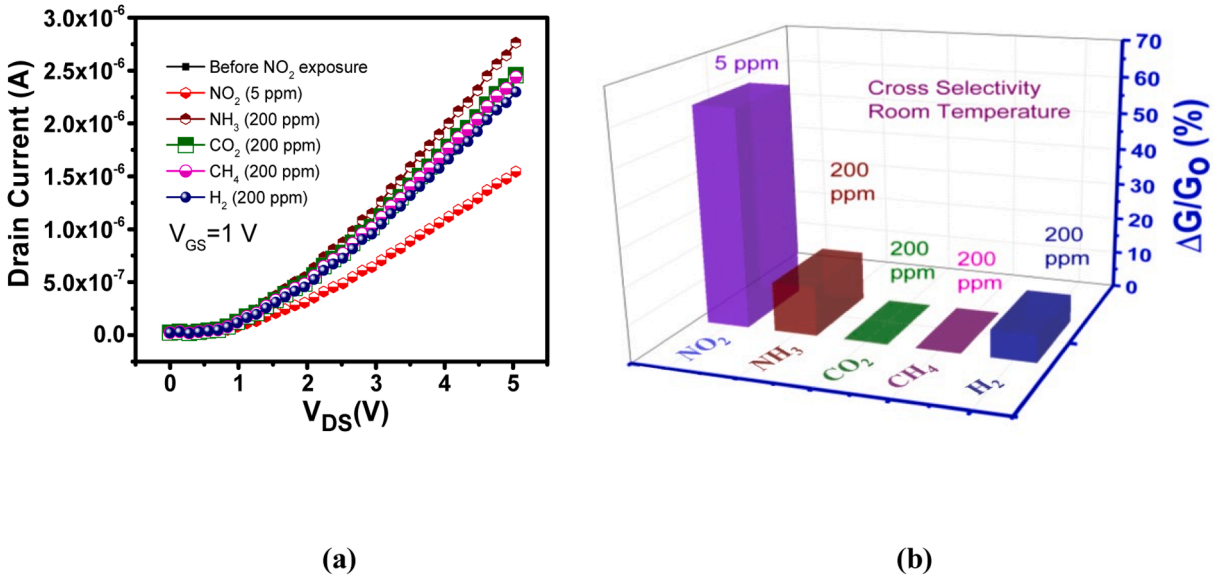

Fig. 14. (a) Output characteristics curves of fabricated four-layer MoS_2 FET obtained for NH_3, CO_2, CH_4 and H_2 gases at 200 ppm, NO_2 at 5 ppm, and (b) histogram for obtained sensor response for different interfering gases.

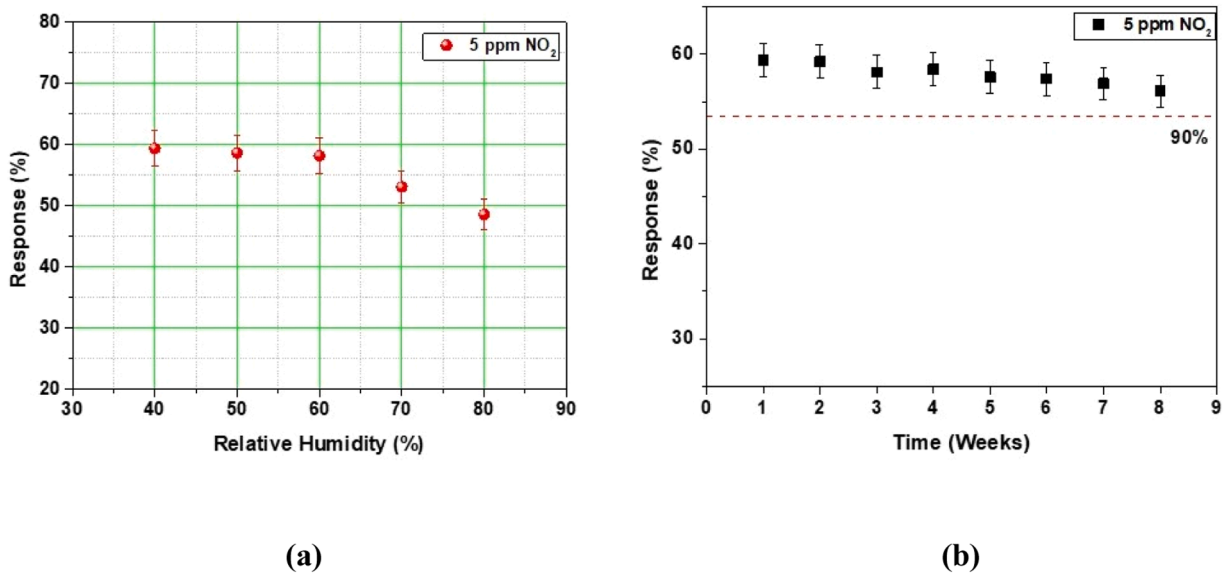

Fig. 15. (a)Effect of humidity on the sensor response and (b)stability of the sensor response towards 5 ppm NO_2.

Table 4
Gas sensing response of different gases for four-layer MoS_2 sensor structure operating at room temperature.

Different gases	Gas concentration (ppm)	Sensor response (%)
NO_2	5	59.4
NH_3	200	13.4
CO_2	200	0.1
CH_4	200	0.16
H_2	200	7.5

at $V_{GS} = 1$ V for ammonia (NH_3), CO_2 (carbon dioxide), methane (CH_4) and hydrogen (H_2) at very high concentration of 200 ppm, whereas corresponding response for target gas (NO_2) of 5 ppm only. All gases were obtained from highly pure (> 99 %) cylinders of gases procured commercially. It is to be noticed that NH_3 being electron donor increases the electron density in the MoS_2 channel and hence increase in the drain current can be noticed towards 200 ppm NH_3 gas. No significant change in the drain current was observed towards other interfering gases. Fig. 14(b) shows the histogram for sensor response obtained for interfering gases where sensor response was calculated using Eq. (6). It can be observed from Fig. 14(b) that fabricated sensor shows the maximum response of 37.2 % even at low concentration of 5 ppm NO_2 gas as compared to sensing response towards other gases of higher concentration of 200 ppm. The effect of humidity and the stability of the sensor were also studied and are displayed in Fig. 15. It is evident from Fig. 15 (a) that up to a relative humidity of 60 %, there is a minor variation in the sensor response towards 5 ppm NO_2, while a higher value of relative humidity (> 60 %) interferes with the sensing behaviour. The stability of the sensor response towards 5 ppm NO_2 was evaluated over a period of 8 weeks and it was found the sensor exhibit a change in response of < 10 % over the 8 weeks as shown in Fig. 15(b).

Table 4 summarizes the sensor response obtained for four-layer MoS_2 sensing structure for various interfering gases at higher concentrations. The obtained result show the possible application of fabricated sensor towards room temperature operated NO_2 gas sensor without

Table 5
Comparison of the sensor with other room temperature 2D materials-based FET sensors for NO_2.

Material	NO_2 concentration (ppm)	Response (%)	Ref
$MoTe_2$	0.001	140	[60]
Graphene	1	6	[61]
$NbSe_2/WSe_2$	5	34	[62]
WSe_2	5	0.4	[63]
MoS_2	200	8	[64]
Black Phosphorus	0.02	20	[65]
MoS_2	5	59.4	Present work

interference with other gases. The fabricated gas sensor was also compared with other 2D materials-based FET sensors operating at room temperature. Although, the $MoTe_2$ based sensor fabricated by Feng et al. shows a higher response, it requires high gate biasing (60 V) in order to obtain proper recovery [60]. The comparison is summarised in Table 5.

4. Conclusions

PLD grown MoS_2 layers were exploited for gas sensing applications using MoS_2 as gas sensing matrix based back gated FETs. Three different thickness of MoS_2, (i) single layer, four-layer, and (ii) ten-layer MoS_2 were chosen to see the significant effect of change in surface to volume ratio on gas sensing performance of the MoS_2 FETs. Schottky contact on MoS_2 layers using Au/Cr is used as source-drain electrodes and output curves and transfer curves were obtained. Systematic gas sensing experiments were carried out from 1 ppm to 500 ppm on fabricated sensor structures i.e. Au/Cr/single layer $MoS_2/Si_3N_4/Si$, Au/Cr/four-layer $MoS_2/Si_3N_4/Si$ and Au/Cr/ten-layer $MoS_2/Si_3N_4/Si$, using output and transfer curves. Effect of NO_2 gas adsorption on MoS_2 was expalined using realignment of energy band diagram. Sensing response (%) for Au/Cr/four-layer $MoS_2/Si_3N_4/Si$ structure was found to be maximum as comapred to the case of single layer and ten-layer. To see the selectivity of optimized Au/Cr/four-layer $MoS_2/Si_3N_4/Si$ sensor structure, sensor was exposed to different interferring gases including NH_3, CH_4, CO_2 and H_2 and it was found that optimized sensor is highly selective towards NO_2 gas.

Availability of data and materials

Not Applicable.

Funding

Not Applicable

CRediT authorship contribution statement

Sujit Kumar: Writing – original draft, Methodology, Investigation, Formal analysis, Data curation, Conceptualization. **Anjali Sharma:** Writing – review & editing, Validation, Supervision, Formal analysis. **Ajay K. Sao:** Investigation. **Jatinder Pal Singh:** Writing – review & editing, Investigation. **Arijit Chowdhuri:** Supervision, Validation. **Monika Tomar:** Writing – review & editing, Validation, Supervision, Resources.

Declaration of competing interest

The authors declare that they have no known competing financial interests or personal relationships that could have appeared to influence the work reported in this paper.

Acknowledgements

Authors are grateful to Late Prof. Vinay Gupta, Department of Physics and Astrophysics, University of Delhi for extending the research facilities and guiding throughout the work. Authors are also thankful to DST for a sponsored research project. One of the authors Sujit Kumar is thankful to the University Grant Commission (UGC), Government of India, Delhi, India for providing research fellowship.

References

[1] S. Kanan, O. El-Kadri, I. Abu-Yousef, M. Kanan, Semiconducting metal oxide based sensors for selective gas pollutant detection, Sensors 9 (10) (Oct. 2009) 8158–8196, https://doi.org/10.3390/s91008158.
[2] X. Fang, B. Zong, S. Mao, Metal–Organic framework-based sensors for environmental contaminant sensing, SpringerOpen (2018), https://doi.org/10.1007/s40820-018-0218-0.
[3] Y.-F. Sun, et al., Metal oxide nanostructures and their gas sensing properties: a review, Sensors 12 (3) (Feb. 2012) 2610–2631, https://doi.org/10.3390/s120302610.
[4] K. Kan, et al., Preparation of Co_3O_4 hollow nanospheres and gas sensing properties, Cailiao Gongcheng J. Mater. Eng. 47 (1) (Jan. 2019) 50–57, https://doi.org/10.11868/j.issn.1001-4381.2017.000114.
[5] J. Kim, K. Yong, Mechanism study of ZnO nanorod-bundle sensors for H_2S gas sensing, J. Phys. Chem. C 115 (15) (Apr. 2011) 7218–7224, https://doi.org/10.1021/jp110129f.
[6] C.C. Li, Z.F. Du, L.M. Li, H.C. Yu, Q. Wan, T.H. Wang, Surface-depletion controlled gas sensing of ZnO nanorods grown at room temperature, Appl. Phys. Lett. 91 (3) (2007), https://doi.org/10.1063/1.2752541.
[7] X. Li, et al., High-performance photoelectrochemical-type self-powered UV photodetector using epitaxial TiO_2 /SnO_2 branched heterojunction nanostructure, Small 9 (11) (Jun. 2013) 2005–2011, https://doi.org/10.1002/smll.201202408.
[8] T. Van Dang, N. Duc Hoa, N. Van Duy, N. Van Hieu, Chlorine gas sensing performance of on-chip grown ZnO, WO_3, and SnO_2 nanowire sensors, ACS Appl. Mater. Interfaces 8 (7) (Mar. 2016) 4828–4837, https://doi.org/10.1021/acsami.5b08638.
[9] M. Shariati, F. Khosravinejad, The laser-assisted field effect transistor gas sensor based on morphological Zinc-excited Tin-Doped $In2O_3$ nanowires, Surf. Rev. Lett. 24 (8) (Dec. 2017), https://doi.org/10.1142/S0218625X1750113X.
[10] E. Moreau, et al., Graphene growth by molecular beam epitaxy on the carbon-face of SiC, Appl. Phys. Lett. 97 (24) (Dec. 2010), https://doi.org/10.1063/1.3526720.
[11] J. Janata, M. Josowicz, Conducting polymers in electronic chemical sensors, Nat. Mater. 2 (1) (Jan. 2003) 19–24, https://doi.org/10.1038/nmat768.
[12] J.J. Miasik, A. Hooper, B.C. Tofield, Conducting polymer gas sensors, R. Soc. Chem. (Jan. 01, 1986), https://doi.org/10.1039/F19868201117.
[13] S. Virji, J. Huang, R.B. Kaner, B.H. Weiller, Polyaniline nanofiber gas sensors: examination of response mechanisms, Nano Lett. 4 (3) (Mar. 2004) 491–496, https://doi.org/10.1021/nl035122e.
[14] M. Bai, et al., An effective strategy for synthesizing high-performance photocatalyst by recycling the graphite target wastes, J. Environ. Chem. Eng. 12 (5) (Oct. 2024) 113872, https://doi.org/10.1016/j.jece.2024.113872.
[15] J. Huang, G. Xie, X. Xu, Z. Geng, Y. Su, Degradable multilayer fabric sensor with wide detection range and high linearity, ACS Appl. Mater. Interfaces 16 (43) (Oct. 2024) 58838–58847, https://doi.org/10.1021/acsami.4c12066.
[16] J. Huang, et al., Hierarchical carbon nanotube-decorated polyacrylonitrile smart textiles for wearable biomonitoring, Wearable Electron. 1 (Dec. 2024) 180–188, https://doi.org/10.1016/j.wees.2024.07.002.
[17] X. Luo, W. Li, L. Yuan, G. Xie, Y. Su, Self-powered infrared detector enabled by interfacial anchoring and thermal reinforcement, Nano Trends 8 (Dec. 2024) 100061, https://doi.org/10.1016/j.nwnano.2024.100061.
[18] Y. Su, et al., Sensing–transducing coupled piezoelectric textiles for self-powered humidity detection and wearable biomonitoring, Mater. Horiz. 10 (3) (2023) 842–851, https://doi.org/10.1039/D2MH01466A.
[19] P. Tyagi, A. Sharma, M. Tomar, V. Gupta, Metal oxide catalyst assisted SnO_2 thin film based SO_2 gas sensor, Sens. Actuators B Chem. 224 (Mar. 2016) 282–289, https://doi.org/10.1016/j.snb.2015.10.050.
[20] J.S. Symanski, S. Bruckenstein, Conductometric sensor for parts per billion sulfur dioxide determination, Anal. Chem. 58 (8) (1986) 1771–1777, https://doi.org/10.1021/ac00121a038.
[21] M. Donarelli, L. Ottaviano, '2D Materials for gas sensing applications: a review on graphene oxide, MoS2, WS 2 and phosphorene', Sensors 18 (11) (Oct. 2018) 3638, https://doi.org/10.3390/s18113638.
[22] A. Ponzoni, et al., Metal oxide gas sensors, a survey of selectivity issues addressed at the SENSOR Lab, Brescia (Italy), Sensors 17 (4) (Mar. 2017) 714, https://doi.org/10.3390/s17040714.
[23] C. Wang, L. Yin, L. Zhang, D. Xiang, R. Gao, Metal oxide gas sensors: sensitivity and influencing factors, Sensors 10 (3) (Mar. 2010) 2088–2106, https://doi.org/10.3390/s100302088.

[24] G.F. Fine, L.M. Cavanagh, A. Afonja, R. Binions, Metal oxide semi-conductor gas sensors in environmental monitoring, Sensors 10 (6) (Jun. 2010) 5469–5502, https://doi.org/10.3390/s100605469.
[25] H. Bai, G. Shi, Gas sensors based on conducting polymers, Sensors 7 (3) (Mar. 2007) 267–307, https://doi.org/10.3390/s7030267.
[26] H. Yoon, Current trends in sensors based on conducting polymer nanomaterials, Nanomaterials 3 (3) (Aug. 2013) 524–549, https://doi.org/10.3390/nano3030524.
[27] K. Cheah, M. Forsyth, V.T. Truong, Ordering and stability in conducting polypyrrole, Synth. Met. 94 (2) (Apr. 1998) 215–219, https://doi.org/10.1016/s0379-6779(98)00006-x.
[28] A. Splendiani, et al., Emerging photoluminescence in monolayer MoS_2', Nano Lett. 10 (4) (Apr. 2010) 1271–1275, https://doi.org/10.1021/nl903868w.
[29] G. Eda, H. Yamaguchi, D. Voiry, T. Fujita, M. Chen, M. Chhowalla, Photoluminescence from chemically exfoliated MoS_2', Nano Lett. 11 (12) (Dec. 2011) 5111–5116, https://doi.org/10.1021/nl201874w.
[30] Y. Yu, C. Li, Y. Liu, L. Su, Y. Zhang, L. Cao, Controlled scalable synthesis of uniform, high-quality monolayer and few-layer MoS_2 films, Sci. Rep. 3 (2013) 1866, https://doi.org/10.1038/srep01866.
[31] M. Donarelli, et al., Response to NO_2 and other gases of resistive chemically exfoliated MoS_2-based gas sensors, Sens. Actuators B Chem. 207 (PartA) (2015) 602–613, https://doi.org/10.1016/j.snb.2014.10.099.
[32] S. Zhao, J. Xue, W. Kang, Gas adsorption on MoS_2 monolayer from first-principles calculations, Chem. Phys. Lett. 595–596 (Mar. 2014) 35–42, https://doi.org/10.1016/j.cplett.2014.01.043.
[33] Q. He, et al., Fabrication of flexible MoS_2 thin-film transistor arrays for practical gas-sensing applications, Small 8 (19) (Oct. 2012) 2994–2999, https://doi.org/10.1002/smll.201201224.
[34] Y. Zhou, G. Liu, X. Zhu, Y. Guo, Ultrasensitive NO_2 gas sensing based on rGO/MoS_2 nanocomposite film at low temperature, Sens. Actuators B Chem. 251 (2) (2017) 280–290, https://doi.org/10.1016/j.snb.2017.05.060.
[35] T. Pham, G. Li, E. Bekyarova, M.E. Itkis, A. Mulchandani, MoS_2 -based optoelectronic gas sensor with sub-parts-per-billion limit of NO_2 gas detection, ACS Nano 13 (3) (2019) 3196–3205, https://doi.org/10.1021/acsnano.8b08778.
[36] D. Wu, et al., Construction of MoS_2/Si nanowire array heterojunction for ultrahigh-sensitivity gas sensor, Nanotechnology 28 (43) (2017), https://doi.org/10.1088/1361-6528/aa89b5.
[37] J. Park, J. Mun, J.S. Shin, S.W. Kang, Highly sensitive two dimensional MoS_2 gas sensor decorated with Pt nanoparticles, R. Soc. Open Sci. 5 (12) (Dec. 2018), https://doi.org/10.1098/rsos.181462.
[38] J. Wang, Q. Zhou, Z. Lu, Z. Wei, W. Zeng, Gas sensing performances and mechanism at atomic level of Au-MoS_2 microspheres, Appl. Surf. Sci. 490 (May) (2019) 124–136, https://doi.org/10.1016/j.apsusc.2019.06.075.
[39] G. Deokar, et al., MoS_2–Carbon nanotube hybrid material growth and gas sensing, Adv. Mater. Interfaces 4 (24) (2017) 1–10, https://doi.org/10.1002/admi.201700801.
[40] H. Li, et al., Fabrication of single- and multilayer MoS_2 film-based field-effect transistors for sensing NO at room temperature, Small 8 (1) (Jan. 2012) 63–67, https://doi.org/10.1002/smll.201101016.
[41] S. Kumar, et al., High performance UV photodetector based on MoS_2 layers grown by pulsed laser deposition technique, J. Alloys Compd. 835 (Sep. 2020) 155222, https://doi.org/10.1016/j.jallcom.2020.155222.
[42] S. Kumar, A. Sharma, M. Tomar, V. Gupta, Realization of low-power and high mobility thin film transistors based on MoS_2 layers grown by PLD technique, Mater. Sci. Eng. B Solid-State Mater. Adv. Technol. 266 (Apr. 2021) 115047, https://doi.org/10.1016/j.mseb.2021.115047.
[43] S. Sinha, et al., Study of band alignment at MoS_2/SiO_2interfaces grown by pulsed laser deposition method, J. Appl. Phys. 129 (11) (Mar. 2021) 115303, https://doi.org/10.1063/5.0039463.
[44] X. Zou, et al., Rational design of sub-parts per million specific gas sensors array based on metal nanoparticles decorated nanowire enhancement-mode transistors, Nano Lett. 13 (7) (Jul. 2013) 3287–3292, https://doi.org/10.1021/nl401498t.
[45] A. Allain, J. Kang, K. Banerjee, A. Kis, Electrical contacts to two-dimensional semiconductors, Nat. Publ. Group (Dec. 01, 2015), https://doi.org/10.1038/nmat4452.
[46] M. Saab, P. Raybaud, Tuning the magnetic properties of MoS_2 single nanolayers by 3d metals edge doping, J. Phys. Chem. C 120 (19) (May 2016) 10691–10697, https://doi.org/10.1021/acs.jpcc.6b02865.
[47] N. Singh, U. Schwingenschlögl, A route to permanent valley polarization in Monolayer MoS_2, Adv. Mater. 29 (1) (Jan. 2017) 1600970, https://doi.org/10.1002/adma.201600970.
[48] W. Li, M. Shahbazi, K. Xing, T. Tesfamichael, N. Motta, D.-C. Qi, Highly sensitive NO_2 gas sensors based on MoS_2@MoO_3 magnetic heterostructure, Nanomaterials 12 (8) (Apr. 2022) 1303, https://doi.org/10.3390/nano12081303.
[49] Y. Kim, et al., Improved sensitivity in Schottky contacted two-dimensional MoS_2 gas sensor, ACS Appl. Mater. Interfaces 11 (42) (2019) 38902–38909, https://doi.org/10.1021/acsami.9b10861.
[50] B. Liu, L. Chen, G. Liu, A.N. Abbas, M. Fathi, C. Zhou, High-performance chemical sensing using Schottky-contacted chemical vapor deposition grown monolayer MoS_2 transistors, ACS Nano 8 (5) (May 2014) 5304–5314, https://doi.org/10.1021/nn5015215.
[51] A. Javey, H. Dai, Carbon nanotube electronics, in: Proceedings of the IEEE International Conference on VLSI Design, 2006, pp. 453–458, https://doi.org/10.1109/VLSID.2006.57.
[52] J. Nah, et al., Quantum size effects on the chemical sensing performance of two-dimensional semiconductors, J. Phys. Chem. C 116 (17) (May 2012) 9750–9754, https://doi.org/10.1021/jp300446z.
[53] X. Cui, M. Freitag, R. Martel, L. Brus, P. Avouris, Controlling energy-level alignments at carbon nanotube/Au contacts, Nano Lett. 3 (6) (Jun. 2003) 783–787, https://doi.org/10.1021/nl034193a.
[54] T.Y. Wei, P.H. Yeh, S.Y. Lu, Z.L. Wang, Gigantic enhancement in sensitivity using Schottky contacted nanowire nanosensor, J. Am. Chem. Soc. 131 (48) (Dec. 2009) 17690–17695, https://doi.org/10.1021/ja907585c.
[55] W. TANG, J. WANG, Enhanced gas sensing mechanisms of metal oxide heterojunction gas sensors, Acta Phys.-Chim. Sin. 32 (5) (2016) 1087–1104, https://doi.org/10.3866/PKU.WHXB201602224.
[56] M.W. Lin, et al., Thickness-dependent charge transport in few-layer MoS_2 field-effect transistors, Nanotechnology 27 (16) (2016) 0, https://doi.org/10.1088/0957-4484/27/16/165203.
[57] D.J. Late, et al., Sensing behavior of atomically thin-layered MoS_2 transistors, ACS Nano 7 (6) (Jun. 2013) 4879–4891, https://doi.org/10.1021/nn400026u.
[58] J. Kong, et al., Nanotube molecular wires as chemical sensors, Science 287 (5453) (Jan. 2000) 622–625, https://doi.org/10.1126/science.287.5453.622.
[59] D. Zhang, et al., Detection of NO_2 down to ppb levels using individual and multiple In2O3 nanowire devices, Nano Lett. 4 (10) (Oct. 2004) 1919–1924, https://doi.org/10.1021/nl0489283.
[60] Z. Feng, et al., Highly sensitive $MoTe_2$ chemical sensor with fast recovery rate through gate biasing, 2D Mater. 4 (2) (Feb. 2017) 025018, https://doi.org/10.1088/2053-1583/aa57fe.
[61] R.K. Paul, S. Badhulika, N.M. Saucedo, A. Mulchandani, Graphene nanomesh as highly sensitive chemiresistor gas sensor, Anal. Chem. 84 (19) (Oct. 2012) 8171–8178, https://doi.org/10.1021/ac3012895.
[62] B. Cho, et al., Two-dimensional atomic-layered alloy junctions for high-performance wearable chemical sensor, ACS Appl. Mater. Interfaces 8 (30) (Aug. 2016) 19635–19642, https://doi.org/10.1021/acsami.6b05943.
[63] F. Ricciardella, et al., Calibration of nonstationary gas sensors based on two-dimensional materials, ACS Omega 5 (11) (Mar. 2020) 5959–5963, https://doi.org/10.1021/acsomega.9b04325.
[64] D.J. Late, et al., Sensing behavior of atomically thin-layered MoS_2 transistors, ACS Nano 7 (6) (Jun. 2013) 4879–4891, https://doi.org/10.1021/nn400026u.
[65] A.N. Abbas, et al., Black phosphorus gas sensors, ACS Nano 9 (5) (May 2015) 5618–5624, https://doi.org/10.1021/acsnano.5b01961.